Antimicrobial ZnO Nanoparticle–Doped Polyvinyl Alcohol/Pluronic Blends as Active Food Packaging Films

Khaled M. Amin,* Abir M. Partila, Hassan A. Abd El-Rehim, and Noha M. Deghiedy

Today, plastic waste has been highlighted as one of the greatest threats to the environment. These environmental concerns and the increased necessity for safe food packaging have inspired scientists to focus on the development of active biodegradable materials. Herein, a novel poly(vinyl alcohol)/pluronic/ZnO nanocomposite film (PVA/PLUR/ZnO) is introduced as an active packaging material with enhanced antimicrobial activity. Gamma irradiation is used as a "green" route to prepare ZnO nanoparticles via a polymer pyrolysis method. The as-prepared ecofriendly ZnO nanoparticles are characterized and incorporated into the PVA/PLUR matrix in different concentrations. Transmission electron microscopy and dynamic light scattering measurements prove that ZnO nanoparticles have a mean particle size of 30 nm with a spherical-like morphology. Morphological and structural characterization confirm the successful incorporation of ZnO into the PVA/PLUR matrix, which in turn enhances the thermal and barrier properties of PVA/PLUR/ZnO nanocomposite films. On the other hand, the opacity of blends is increased. The PVA/PLUR/ZnO composites exhibit broad-spectrum antimicrobial activity against Gram-positive, Gram-negative bacterial pathogens, and fungi, and the activity increases with increasing concentrations of ZnO nanoparticles. These results introduce PVA/PLUR/ZnO films as effective antimicrobial materials for active food-packaging applications.

K. M. Amin
Department of Materials Science
Technische Universität Darmstadt
Darmstadt 64287, Germany
E-mail: amin@ma.tu-darmstadt.de, khaledamin89@gmail.com
K. M. Amin, Prof. H. A. Abd El-Rehim, Dr. N. M. Deghiedy
Department of Polymer Chemistry
Atomic Energy Authority
Cairo 11787, Egypt
Dr. A. M. Partila
Department of Radiation Microbiology
Atomic Energy Authority
Cairo 11787, Egypt

The ORCID identification number(s) for the author(s) of this article can be found under https://doi.org/10.1002/ppsc.202000006.

1. Introduction

In the last few decades, environmental concerns and problems regarding plastic waste have increases with the strong desire to improve the living conditions worldwide; thus, the utilization of biodegradable and antimicrobial polymeric films has attracted substantial attention in the packaging industry.[1,2] The increased demand for "ready to eat" food had made consumers and the manufacturers more aware of the potential hazards associated with packaging materials. Innovations in food packaging include the development of active packaging solutions based on natural active compounds aimed at increasing both the shelf-life of the packed food and the sustainability of the overall product.[3] Unlike ordinary food containers, active packaging materials are specifically designed to reduce the permeability to oxygen or moisture, to protect the food from exposure to heat and light, while the intelligent packaging serves as sensors interacting with the food and providing information on potential deterioration or contamination. In recent decades, the biodegradable films have been considered and developed by many researchers; however, their applications in the food packing industry suffer from some constraints such as frangibility because of low mechanical strength and poor inhibition of gas exchange.[4]

Foodborne pathogens are considered as one of the major reasons for hospitalizations, human beings' illnesses, and deaths every year. In the food market, the proliferation of pathogens takes place on the surface and packaging of foods. In terms of downgraded or lost products, the millions of dollars as the microbiological costs of contamination are being paid by the food industry.[5] Among people, *Toxoplasma gondii*, *Staphylococcus aureus*, *Campylobacter* spp., *Escherichia coli*, and *Salmonella* spp. are considered as the top sources of pathogens that lead to foodborne and illness death.[6]

Over the past decade, the growing use of nanomaterials in nearly all fields has opened the door for their application as packaging materials.[7] Nanotechnology-enhanced packaging materials can work through two mechanisms of action. The first one is improved packaging, as the uniform dispersion of nanofillers into a polymer matrix result in a high matrix/filler interfacial area, which confines the mechanical mobility
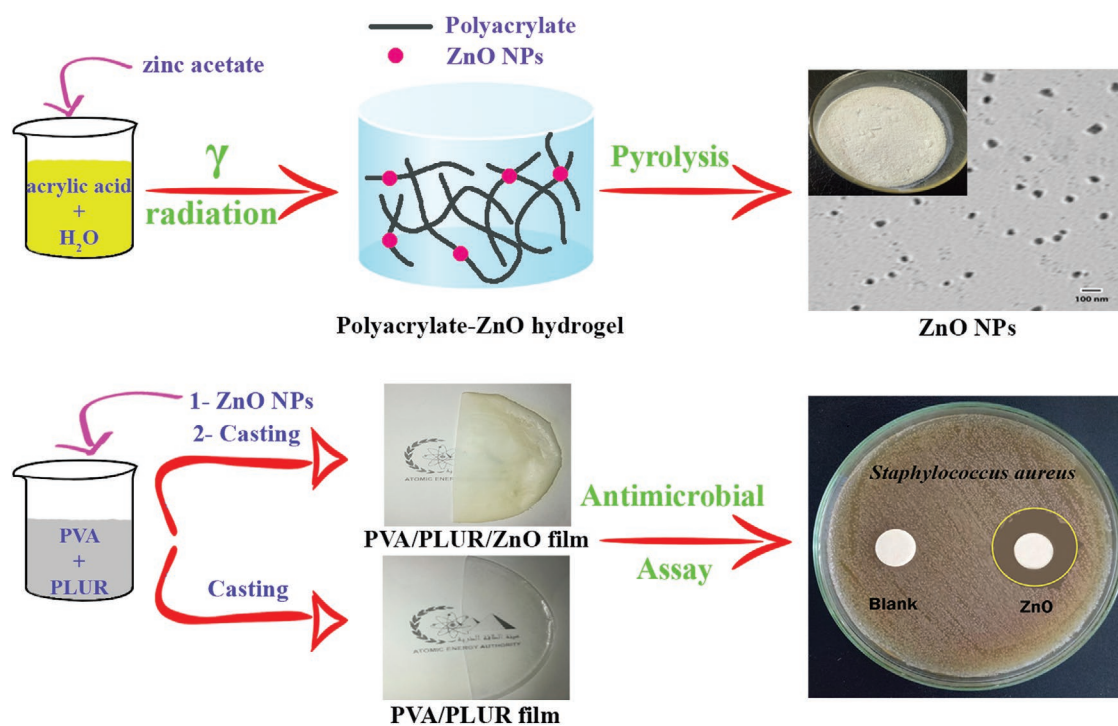
Figure 1. Schematic illustration showing the fabrication process of the ZnO nanoparticles and the formation of the PVA/PLUR/ZnO nanocomposite films.

of the matrix, and improves its mechanical, thermal, and barrier properties.[8,9] The second mechanism is active packaging, as the nanofillers directly interact with the packed food or its environment and offer enhanced food protection. In this regard, zinc oxide (ZnO) nanostructured materials have found various applications in everyday life such as in drug delivery, cosmetics, and medical devices due to their strong antimicrobial effects on a board range of microorganisms.[10,11] Moreover, ZnO is currently listed by the Food and Drug Administration (FDA) as a generally recognized as safe (GRAS) material.[12] Several techniques such as chemical vapor deposition (CVD),[13] solution precipitation,[14] thermal decomposition,[15] hydrothermal preparation,[16] spray pyrolysis,[17] polymer pyrolysis,[18] and sol-gel method,[19] have been employed to prepare ZnO. Gamma irradiation offers a promising eco-friendly route for low-cost and large-scale production of metal oxides at ambient condition. Furthermore, the irradiation-induced reduction does not involve catalyst precursors or reducing agents which offers a production process without any chemical requirements or waste streams.[9,20] Combining gamma irradiation with polymer pyrolysis provides a simple, reproducible, inexpensive, nonvacuum, and low energy consuming process for preparing ZnO nanoparticles. Earlier studies[21,22] have investigated the optimization of conditions of ZnO preparation via polymer pyrolysis route, thus, the composition of zinc acetate and acrylic acid has been previously reported.

The synthesis of ZnO nanoparticles via the polymer pyrolysis is based on the polymerization of acrylic acid in the presence of a ZnO precursor to obtain ZnO polyacrylate using a chemical initiator in an intermediate stabilization step in the preparation.[23] The chemical initiator oxidizes the monomer, enhancing the linking between monomers. Recent concern

has been paid regarding the use of gamma radiation instead of chemical initiators in polymer pyrolysis because it generally yields highly pure materials through an environmentally friendly and economically viable process. Although several reports on ZnO-based nanocomposite biopolymers have appeared in the literature,[10,24,25] a few of them have focused on polyvinyl alcohol (PVA) and pluronic (PLUR), which are degradable polymers suitable for food packaging.

To the best of our knowledge, the use of gamma radiation in polymer pyrolysis for the preparation of ZnO incorporated into nanocomposite films for food packaging is a novel approach. Moreover, the structure, thermal and barrier properties, and surface morphologies of the as-synthesized ZnO nanoparticles, the PVA/PLUR blend and the nanocomposite films (PVA/PLUR/ZnO) were studied. Herein, we use the most promising multifunctional PVA/PLUR blends immobilized with ZnO nanoparticles prepared in an eco-friendly manner to develop antimicrobial polymer films with broad zone of inhibitory activity against Gram-positive bacteria (*Bacillus subtilis* and *Staphylococcus aureus*), Gram-negative bacteria (*Escherichia coli* and *Pseudomonas aeruginosa*) and fungi (*Candida albicans*). Critically, we examined the film permeability and antimicrobial activity variations, which are crucial in a wide range of packaging applications for enhancing food safety and shelf life. **Figure 1** summarizes the different processes and techniques used in this study.
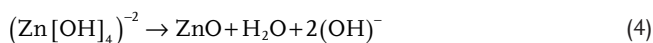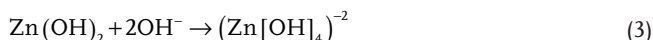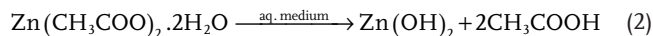
2. Results and Discussion

Starting with zinc acetate as the Zn precursor, ZnO nanoparticles were synthesized by mixing appropriate amount of Zn acetate with an aqueous solution of acrylic acid. Gamma radiation was

2000006 (2 of 11)

**ADVANCED
SCIENCE NEWS**
www.advancedsciencenews.com

Particle
& Particle Systems Characterization
www.particle-journal.com

then used as the initiator of the polymerization reaction to transform the precursor into eco-friendly ZnO nanoparticles.

When the aqueous solution was irradiated with γ-rays, the radiolysis of water produced many active species such as e^-_{aq}, $H^\cdot$ and $\cdot OH$ (Equation (1)).[26]

$$H_2O \xrightarrow{\text{Gamma radiation}} e^-_{aq}, H^\cdot, HO^-, OH^\cdot, H_3O^+, H_2, H_2O_2 \qquad (1)$$
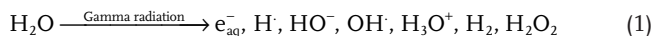
The generated species reduce the formed $Zn(OH)_2$ leading to the development of $(Zn[OH]_4)^{2-}$ and ZnO nuclei are formed, which agglomerate into ZnO nanoparticles according to the following mechanism (Equations (2)–(4)).[27]

$$Zn(CH_3COO)_2 \cdot 2H_2O \xrightarrow{\text{aq. medium}} Zn(OH)_2 + 2CH_3COOH \qquad (2)$$

$$Zn(OH)_2 + 2OH^- \rightarrow (Zn[OH]_4)^{-2} \qquad (3)$$

$$(Zn[OH]_4)^{-2} \rightarrow ZnO + H_2O + 2(OH)^- \qquad (4)$$

The Zn^{+2} ions are bound by the strong ionic bonds between the metallic ions and the carboxylate ions in the polymeric chain or between the polymeric chains. This uniform immobilization of metallic ions in the polymer chains favors the formation of uniformly distributed solid solution of the metallic oxides in the pyrolysis process. The resultant ZnO nanoparticles showed an average diameter of 33 nm with narrow size distributions as described below. The ZnO nanocomposite layer was built by the formation of a Zn–O network including dipolar bonding of the Zn with the –OH functional groups in the PVA/PLUR blend as indicated in **Figure 2**. Different surface and structural characterization techniques were used ensure the successful preparation of the eco-friendly ZnO nanoparticles and PVA/PLUR (blank film). To evaluate the successful incorporation of ZnO nanoparticles into the polymer matrix, these analyses were also performed on the blank PVA/PLUR film loaded with 5, 10, 15, 20, and 25 wt% ZnO (Supporting Information). For comparison, data of the blend with the highest antimicrobial activity (25 wt% ZnO) has been shown and represented in the manuscript as (PVA/PLUR/ZnO).

2.1. X-Ray Diffraction Studies

The X-ray diffraction (XRD) patterns of the as-prepared ZnO nanopowder, PVA/PLUR, and PVA/PLUR/ZnO nanocomposite films are presented in **Figure 3**. For the ZnO nanoparticles, the XRD pattern confirms its crystalline nature. The diffraction peaks located at 31.84°, 34.52°, 36.33°, 47.63°, 56.71°, 62.96°, 68.13°, and 69.18° were matched with the hexagonal wurtzite phase of ZnO.[28,29] The peaks are sharp, which indicates the high crystallinity and ultrafine nature of the crystallites. No peaks of impurities were detected, suggesting that high-purity ZnO was obtained. In order to ensure the successful formation of ZnO during the gamma irradiation process, XRD pattern of gamma irradiated ZnO without acrylic acid was employed. It exhibited all the characteristic peaks corresponding to ZnO (Supporting Information S1). XRD pattern for PVA/PLUR blank film shows two sets of diffraction peaks corresponding to PVA and PLUR. The pattern is characteristic of an amorphous phase with the main halo of the typical peak at 2θ of 17.7° and another low intensity peak at 2θ of 20.2°.[30]

The XRD spectrum of the PVA/PLUR/ZnO nanocomposite clearly exhibits peaks characteristic of ZnO nanoparticles in addition to the main amorphous peaks associated with the PVA/PLUR film confirming the incorporation of these nanoparticles into the nanocomposite films. Neither a new peak nor a peak shift compared with pure PVA/PLUR were observed, indicating that the PVA/PLUR/ZnO biocomposite films consisted of two phases, that is, polymer and nanoparticles. These observations show that the addition of ZnO caused an increase in the overall crystallinity of the PVA/PLUR polymer blend, which has a substantial effect on the final proprieties of these biocomposites films. The crystallinity of the polymeric matrix can be enhanced with addition of ZnO nanoparticles, because of the crystalline phases of the biodegradable polymer show
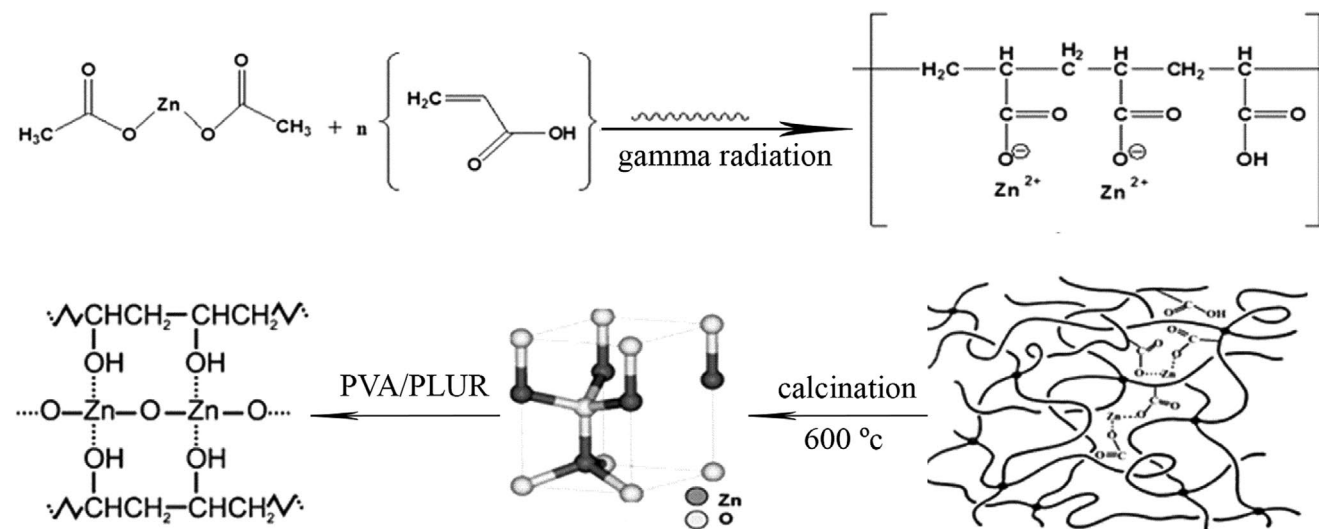

Figure 2. Schematic illustration of the preparation mechanism of the PVA/PLUR/ZnO nanocomposite films.
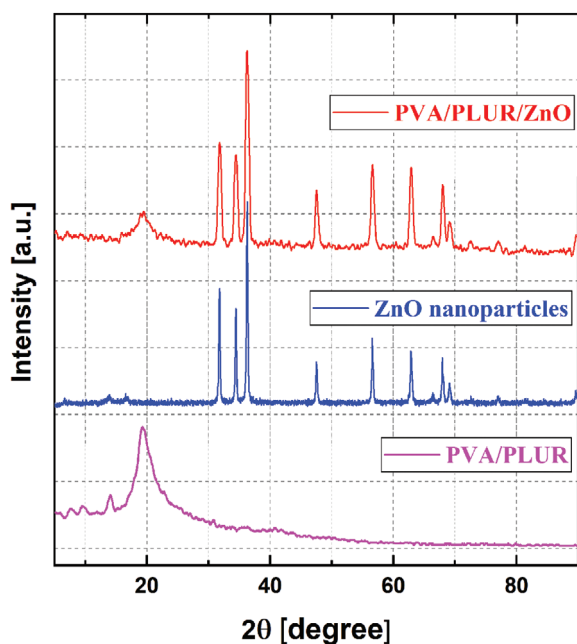
Figure 3. XRD patterns of ZnO, PVA/PLUR, and the PVA/PLUR/ZnO nanocomposite of 25 wt% ZnO.

higher resistance to the hydrolytic degradation exerted by ZnO nanoparticles compared to amorphous ones and the chains are shortening progressively during the hydrolytic degradation; hence, the highly ordered crystalline phase is increased not only because of the increased mobility of the chains but also, the decrease in molecular entanglement.[31] The XRD patterns of all PVA/PLUR/ZnO with different ZnO contents are depicted in Supporting Information S2. They confirmed the incorporation of ZnO in PVA/PLUR blend. They clearly exhibited characteristics peaks corresponding to PVA, PLUR, and ZnO.

2.2. Thermogravimetric Analysis

The thermal properties of the prepared nanocomposite films are considered the most important characteristic for packaging applications especially in food packaging. Melting point (T_m) is the main characteristic that can be used to evaluate thermal properties of the films, which in turn affects the associated enthalpy of fusion. Thus, thermogravimetric analysis (TGA) is very important not only for construction of the films and judging the composing materials but also, evaluating the thermal stability of the fabricated (PVA/PLUR/ZnO) nanocomposite films and their behavior as packaging materials. TGA of PVA/PLUR and PVA/PLUR/ZnO with different concentrations of ZnO were assessed and are displayed in **Figure 4**.

For the blank PVA/PLUR film, the first minor loss at approximately 100 °C is attributed to the evaporation of water in the polymer blend. The second stage, corresponding to a lower percentage of weight loss and includes the melting point of PLUR, is the first decomposition step, and this decomposition may be due to splitting or volatilization of small molecules and continued evaporation of moisture. The decomposition region of the curve, which starts at approximately 300 °C,
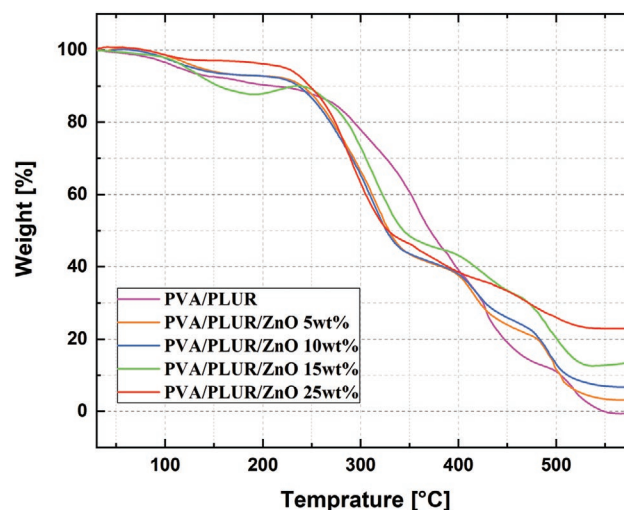

Figure 4. TGA thermograms of ZnO, PVA/PLUR, and the PVA/PLUR/ZnO nanocomposites with different ZnO contents.

covers a wider temperature range that includes the melting point of PVA. The latter process in the TGA curve, which is the main decomposition step, is associated with a significant percentage weight loss.[32]

The TGA curve of the PVA/PLUR/ZnO nanocomposite film shows that the weight loss of the nanocomposite film was lower than that of the pure PVA/PLUR film. Therefore, the PVA/PLUR/ZnO nanocomposite film is more thermally stable than the pure PVA/PLUR film. In general, the incorporation of ZnO nanoparticles into PVA/PLUR blend leads to an increase in thermal stability of polymeric matrix which is in direct correlation with the concentration of nanoparticles. Therefore, as the ZnO content increases, the thermal stability for the blend increases.

The difference in the thermal stability of the bio-nanocomposite films can be explained as follows: The presence of ZnO in the PVA/PLUR matrix and its interactions with the polymer matrix could restrict the motion of the polymer chains or act as a thermal insulator and barrier to the volatile products formed during degradation, leading to a delay in thermal decomposition.[33] On the other hand, as a semiconductor, ZnO can generate free oxygen and oxygen vacancies in the lattice structure by thermal stimulation. The oxygen vacancies can absorb electrons to generate active catalytic positions in the ZnO, and free oxygen enhances the formation of peroxy radicals, which can break the polymer chains.[34] Therefore, the formation of free oxygen and oxygen vacancies dramatically influences polymer decomposition. The above two effects conflict with each other, and the thermal catalysis effect of the ZnO nanoparticles is dominant in most biocomposites.

2.3. Fourier-Transform Infrared Measurements

Fourier-transform infrared (FT-IR) spectroscopy was utilized to evaluate the as-prepared polymer composite films. **Figure 5** presents the FT-IR spectra of the PVA/PLUR (blank film) and PVA/PLUR/ZnO nanocomposite films acquired from 400 to 4000 cm^{-1} wavenumbers, and the spectra show characteristic bands of the

**ADVANCED
SCIENCE NEWS**

www.advancedsciencenews.com

Particle
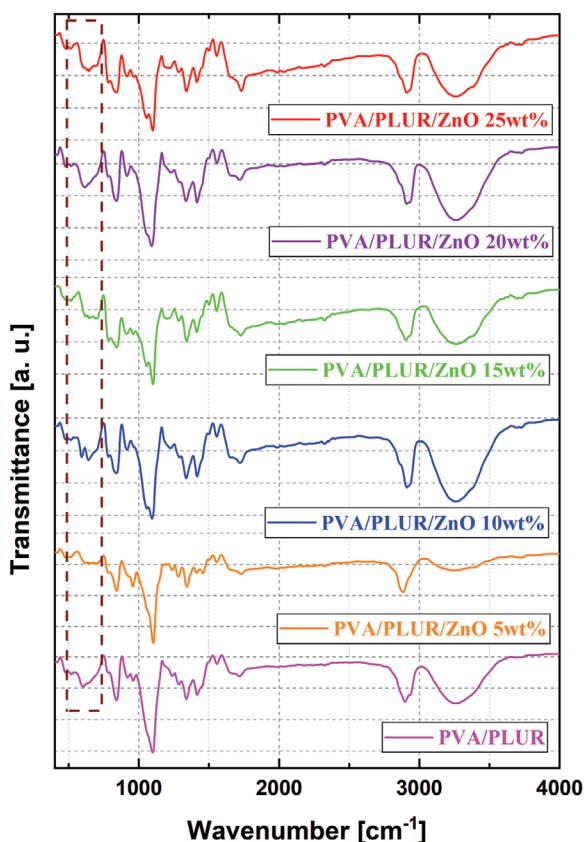& Particle Systems Characterization

www.particle-journal.com

Figure 5. FT-IR spectra of PVA/PLUR and the PVA/PLUR/ZnO nanocomposites with different ZnO contents.

functional groups in the films and the interactions between ZnO nanoparticles and the PVA/PLUR film. Both spectra show the same major bands, which are attributed to the two polymers. In the spectrum of the PVA/PLUR film, a broad band at approximately 3270 cm^{-1} is observed and can be attributed to the stretching of hydroxyl groups.[35] The moderate absorption band at 1417 cm^{-1} corresponds to the CH$_2$ scissoring vibrational mode, and the band at 1659 cm^{-1} is attributed to the O–H bending mode of the hydroxyl groups. The bands at 2896 and 2929 cm^{-1} are due to the C–H stretching modes of –CH and –CH$_2$ of the polymer backbone, respectively.[36,37] The strong absorption band at 1089 cm^{-1} is from the C–O–C stretching vibration of the ether groups in the PLUR and PVA moieties.[38] The band at 844 cm^{-1} corresponds to the CH$_2$ rocking vibrational mode, while the band at 602 cm^{-1} may arise from residual carbonate, which is usually observed in FT-IR spectra acquired in air.

On the other hand, the spectra of the PVA/PLUR/ZnO nanocomposite with varying ZnO content clearly show the major bands associated with the PVA/PLUR film. Moreover, the band correlated with the Zn–O stretching vibration of the ZnO nanoparticles appears at 474 cm^{-1}, which verifies the loading and successful incorporation of these nanoparticles into the polymer matrix.[39,40] However, by increasing the ZnO wt%, the intensity of this band is still very low compared to the other peaks.[41] Moreover, it is overlapped with other peaks in the same area, so it is very difficult to use the peak intensity as a quantitative tool for elucidating the ZnO content. It can only be used as a qualitative

indicator for the incorporation of ZnO nanoparticles in the polymer matrix. FT-IR spectra of the nanocomposites with different ZnO films show no significant change or shift in the characteristic peaks of PVA/PLUR with the addition of ZnO nanoparticles, which is in accordance with the literature.[42,43] However, the variation in intensity and position of bands appeared between 510 and 750 cm^{-1}, which are assigned to the stretching vibration of ZnO, confirms the inclusion of ZnO into PVA/PLUR/ZnO films.[44] On comparing the spectra of PVA/PLUR/ZnO nanocomposites with different ZnO contents, the slight change in broadening of band at 3200–3400 cm^{-1} indicates the formation of more hydrogen bonds between PVA/PLUR and ZnO nanoparticles.[43]

2.4. Morphological Study

Representative transmission electron microscopy (TEM) micrographs of the as-synthesized ZnO, PVA/PLUR, and PVA/PLUR/ZnO composites are presented in **Figure 6**. The ZnO nanoparticles deposited from a dilute aqueous suspension appear as spherical like structures (Figure 6a,b). The individual particles that appear in the micrograph possess diameters that vary from 20 to 40 nm confirming that the as-prepared nanoparticles are monodisperse morphologically homogeneous. These results are in a good agreement with the data obtained from dynamic light scattering (DLS) analysis in which the mean particle size of the ZnO nanoparticles is 34 nm (Figure 6c). This figure shows the particle size distribution of the eco-friendly ZnO nanoparticles and the data analysis indicates that the size distribution is between 30 and 60 nm. However, the percentage of nanoparticles with diameters greater than 50 nm is very low, and the largest fraction of the nanoparticles present in the solution are approximately 35 nm. This figure confirms that the nanoparticles in solution are monodisperse and are uniform in size, which is in good agreement with the results obtained from TEM analysis. As shown in Figure 6d, a flake network-like structure was observed for neat films of the PVA/PLUR blend, whereas micrographs of PVA/PLUR/ZnO (Figure 6e,f) show that the ZnO nanoparticles (black spots) were evenly distributed throughout the blend verifying their incorporation into the PVA/PLUR blend. The ZnO nanoparticles embedded in the polymer matrix appear well dispersed and spherical.

2.5. Color and Opacity Index of the Films

The transparency and color of films are essential parameters for the appearance of food packages and customer acceptance. The opacity index is used to determine the film transparency. As the opacity of a film increases, the transparency decreases. The light absorption of the films was employed to evaluate their transparency. The transparency can be quantified via the opacity index according to Equation (5)[45] and the results are tabulated in **Table 1**:

$$\text{Opacity index} = \frac{\text{Abs}_{600}}{X} \tag{5}$$

where X is the film thickness (mm) and Abs$_{600}$ is the absorbance at 600 nm.
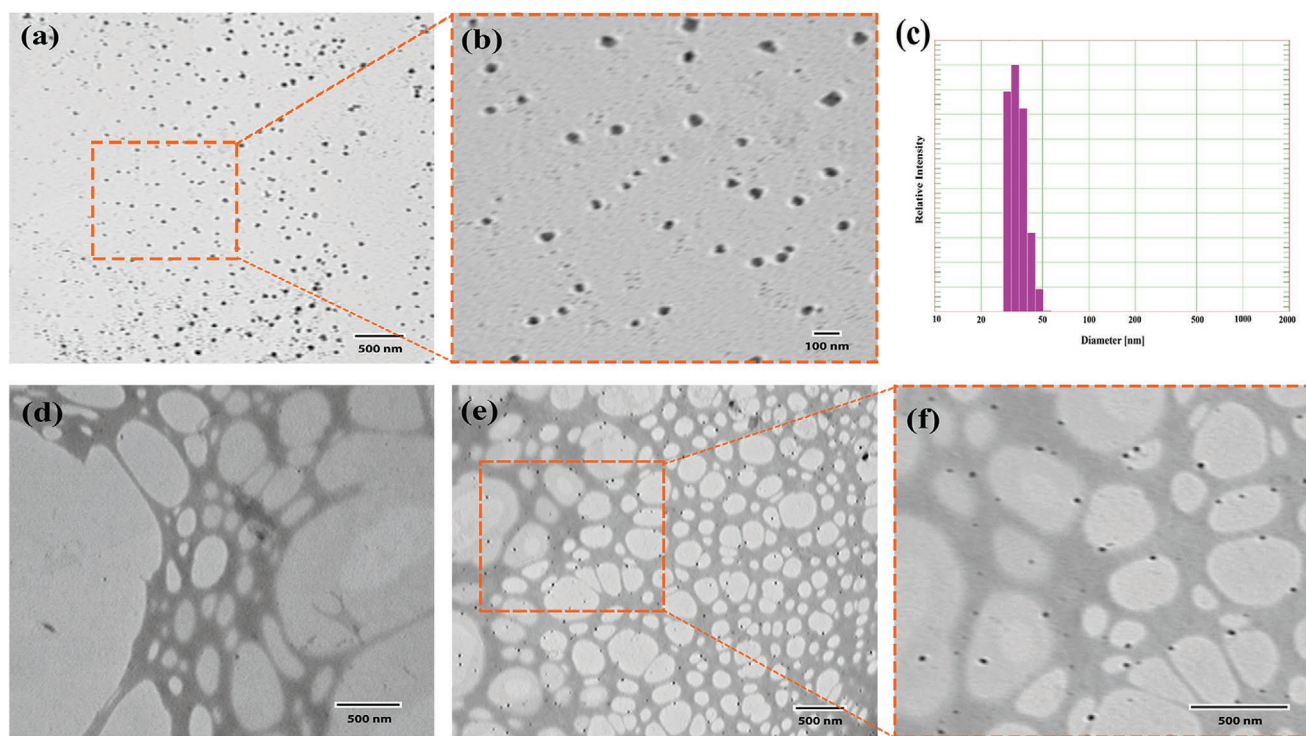
Figure 6. a,b) TEM micrograph of ZnO; c) DLS result for ZnO; TEM micrograph of d) PVA/PLUR blend and e,f) PVA/PLUR/ZnO nanocomposite of 25 wt% ZnO.

As shown in Table 1, the blank PVA/PLUR film shows high transparency, and the opacity index of the blank PVA/PLUR film nearly doubled upon addition of 25 wt% ZnO (from 1.07 to 2.31). The incorporation of the ZnO nanoparticles into the polymer matrix and the thickness of the films led to an increase in opacity due to the decrease in the amount of light passing through the films. As indicated in **Figure 7**a, PVA/PLUR is transparent; consequently, the reduction in film transparency after the addition of ZnO nanoparticles could be attributed to the agglomeration of these nanoparticles in the polymer matrix, which was confirmed by the TEM micrographs. These observations indicate that the ZnO nanoparticles in the polymer matrices block the passage of UV light (Figure 7b); hence, these films can offer a reasonable UV prevention ability without sacrificing transparency completely in case of using lower and optimized concentrations of ZnO, which in turn makes these materials promising alternatives for use in food packaging in conjunction with UV screening.

The calculated RGB color parameters of the images were calculated using MATLAB 2016 software. To better understand color changes accompanying the incorporation of the ZnO nanoparticles, these parameters were converted to other color functions, namely, $L*$ (lightness), $a*$ (red/green), and $b*$ (yellow/blue). The color difference (ΔE), which indicates the degree of total color difference from the standard color plate, was calculated with regard to the color plate parameters ($L = 94.63$, $a = -0.88$, $b = 0.65$) by using the following equation (Equation (6))[46]:

$$\Delta E = \sqrt{\left(\Delta L^*\right)^2 + \left(\Delta a^*\right)^2 + \left(\Delta b^*\right)^2} \tag{6}$$

The values of $L*$, $a*$, $b*$, and ΔE in the pure PVA/PLUR blank film and the PVA/PLUR/ZnO nanocomposite film with different nano-ZnO concentrations and different thicknesses are shown in Table 1. The ΔE value of the pure PVA/PLUR film significantly increased with the incorporation of ZnO nanoparticles into the polymer matrix. The color properties of the blank biopolymer film were affected by the incorporation of ZnO nanoparticles. The $L*$ values decreased slightly, while the $b*$ values increased significantly (three times higher) upon addition of ZnO. This result confirms the increase in the yellowness and greenness of the films and consequently the decrease in the film lightness after the formation of PVA/PLUR/ZnO films with the addition of ZnO nanoparticles. These trends in $L*$ and $b*$ reflect the greater yellow color in the prepared nanocomposite, which was likely caused by the nanoparticles. The total color difference (DE) of the prepared PVA/PLUR/ZnO nanocomposite increased relative to that of the blank PVA/PLUR films.

Table 1. Color parameters and opacity of PVA/PLUR and PVA/PLUR/ZnO nanocomposite films.

Film	$L*$	$a*$	$b*$	ΔE	Thickness [μm]	Opacity
PVA/PLUR	84.5978	−2.5381	3.6349	10.6018	90	1.0736
PVA/PLUR/ZnO	78.8705	−4.3485	12.4512	19.9882	100	2.3082

Figure 7. Photographs of a) the PVA/PLUR blank film and b) the PVA/PLUR/ZnO nanocomposite film of 25 wt% ZnO.

2.6. Oxygen Transmission Rate

Oxygen is the key player in most biological and chemical changes that occur in oxygen-sensitive products and is responsible for food spoilage, which causes flavor changes, rancid oil formation, and mold growth. Hence, the development of active packaging techniques that can lower the oxygen exposure rate of foods and even non-food products that can be harmed by exposure to oxygen to prolong their shelf lives is of great interest to researchers. In this context, the oxygen transmission rate (OTR) was measured for both PVA/PLUR and PVA/PLUR/ZnO to compare their efficiencies as oxygen barriers. In general, thicker packaging films show better barrier properties. On the other hand, increasing the film thickness is restricted by preparation conditions and cost limitations. Hence, combining functional layers allows the preparation of a good barrier film with the properties required to afford a serviceable package.[47] PVA/PLUR showed an OTR of 1230 mL m^{-2} per day, while that of PVA/PLUR/ZnO was 710 mL m^{-2} per day. OTR values are relatively high, however, the PVA/PLUR/ZnO films can still be classified as moderate transmitters.[48] Based on the literature survey, many polymeric packaging materials exhibit high OTR values and can be used for packaging of specific food products.[7] However, the enhancement in the barrier properties of the synthesized PVA/PLUR films introduced upon incorporation of ZnO confirms the synergistic effect of ZnO nanoparticles.[49]

The transmission rate of the PVA/PLUR/ZnO nanocomposite film was substantially lower, that is, by 43%, than that of the blank PVA/PLUR film. This positive correlation between the film structure and its OTR suggests that the incorporation of ZnO nanoparticles into the polymer matrix reduces the intermolecular spaces within the film and creates a tortuous pathway for oxygen penetration, hindering its permeability and enhancing the efficiency of the film as a packaging material.[50] This hindrance can be attributed to the fact that the ZnO nanoparticles are well suited to filling the empty spaces within the films due to their small size.

2.7. Antimicrobial Assay

In the last few years, metal and metal oxide nanoparticles have been shown to have potent antimicrobial activity due to their large surface area to volume ratio, which allows the binding of many ligands on their surface. Among these nanoparticles, ZnO nanoparticles have shown exceptional antimicrobial activities and have been used in a wide range of applications for food protection and agricultural safety.[51] In this study, ZnO nanoparticles were added to blank PVA/PLUR films to enhance their antimicrobial activity. The prepared PVA/PLUR/ZnO nanocomposite films were used as bifunctional materials for food packaging with antimicrobial effects. This is the first study to report the promising and enhanced activity of biodegradable PVA/PLUR/ZnO films as antimicrobial agents against foodborne pathogens, especially *Escherichia coli*, which is considered one of the most important foodborne pathogens in the food industry.[52] This pathogen causes inflammation of the colon, leading to diarrhoea and abdominal pain with bloody stools. The synergistic effects of different concentrations of ZnO nanoparticles (5, 10, 15, 20, and 25 wt%) were evaluated by measuring the clear zone of inhibition (ZOI) against pathogenic Gram-positive (*Bacillus subtilis* and *Staphylococcus aureus*), Gram-negative (*Escherichia coli* and *Pseudomonas aeruginosa*) strains and a fungus (*Candida albicans*).

The results in **Table 2** show that the antimicrobial activity can be observed against all strains under study at all ZnO concentrations, with ZOI values between 15 and 40 mm in diameter. The highest activity was recorded against *Candida albicans* (with 40 mm ZOI), followed by that against the Gram-positive strain *Staphylococcus aureus* (35 mm ZOI). On the other hand, the weakest growth inhibition was against the Gram-negative strain *Pseudomonas aeruginosa* (18 mm). These results show the enhanced biocidal activity for PVA/PLUR/ZnO compared to the previous results for ZnO nanoparticles reported by Tayel et al.,[53] which were an 18 mm ZOI for *Escherichia coli O157:H7*, a 17 mm ZOI for *Pseudomonas aeruginosa* and a 31 mm ZOI for *Staphylococcus aureus*, confirming the synergistic effects between ZnO nanoparticles when added to the PVA/PLUR blend in terms of their antibacterial activity.

Moreover, the results in Table 2 reveal that the inhibition efficiency against all microbial strains under study increases with increasing the concentration of ZnO nanoparticles from 5 to 25 wt% in the PVA/PLUR/ZnO samples, and all the strains

Table 2. Effect of different concentrations (5–25 wt%) of ZnO NPs immobilized on filter paper discs on the growth of different microbial strains cultured on LB agar after 24 h of incubation at 37 °C (filter paper disc size = 10.0 mm).

Strains	ZOI [mm]				
	5 wt%	10 wt%	15 wt%	20 wt%	25 wt%
Escherichia coli	16.0 ± 0.20[a)]	16.0 ± 0.00[b)]	16.0 ± 0.20[b)]	20.0 ± 0.20[b)]	20.0 ± 0.00[c)]
Bacillus subtilis	15.0 ± 0.20[a)]	15.0 ± 0.00[a)]	17.0 ± 0.20[b)]	17.0 ± 0.20[b)]	20.0 ± 0.20[c)]
Candida albicans	30.0 ± 0.20[a)]	32.0 ± 0.00[a)]	35.0 ± 0.20[b)]	38.0 ± 0.20[c)]	40.0 ± 0.00[c)]
Pseudomonas aeruginosa	13.0 ± 0.20[a)]	13.0 ± 0.10[a)]	13.0 ± 0.00[b)]	15.0 ± 0.00[c)]	18.0 ± 0.10[c)]
Staphylococcus aureus	26.0 ± 0.00[a)]	28.0 ± 0.20[b)]	30.0 ± 0.10[c)]	35.0 ± 0.00[d)]	35.0 ± 0.00[d)]

Values are means ± SD ($n = 3$). Data within the groups are analyzed using one-way analysis of variance (ANOVA) followed by [a–f)]Duncan's multiple range test (DMRT) at $p = 0.05$.

were most sensitive to the highest concentration (25 wt%) of ZnO. *Pseudomonas aeruginosa* had the greatest increase in ZOI (38.4%) as the ZnO nanoparticle concentration increased from 5 to 25 wt%, and this result may be due to the better diffusion of nanoparticles into the agar medium. For this reason, in this study, the bacterial counts for the abovementioned strains were determined and the effect of 5 wt% ZnO nanoparticles on the bacterial count was evaluated by counting the number of cell-forming units (CFUs) on the plates (**Table 3**). The microbial counts on LB agar demonstrated that Gram-positive bacteria were generally more sensitive to ZnO nanoparticles than Gram-negative bacteria, and a reduction in the colony counts to 10×10^1 was observed after 24 h of incubation for *Candida albicans* and *Staphylococcus aureus*. The size of the inhibition zone indicates the sensitivity of the pathogen. Gram-positive bacteria showed larger inhibition zones than Gram-negative bacteria. **Figure 8** shows the ZOI of blank and 5 wt% ZnO against *Staphylococcus aureus*, a Gram-positive bacterium, compared to that against *Escherichia coli*, a Gram-negative bacterium. The antimicrobial activity of the ZnO nanoparticles relies on the structure of the bacterial cell wall. Gram-positive bacteria have a thick cell wall consisting of multiple layers of peptidoglycans, whereas Gram-negative bacteria have a complex cell wall consisting of a thin peptidoglycan layer packed by the outer membrane.[46] In the case of Gram-positive bacteria, ZnO nanoparticles interact with the outer layers of the cell wall, which has a large number of pores, providing a facile pathway for the ZnO nanoparticles to penetrate the cells and facilitate leakage of the intracellular contents, ultimately causing cell death. In the case of Gram-negative bacteria, these nanoparticles interact with the outer bacterial membrane first. That membrane is full of phospholipids, lipopolysaccharides and lipoproteins, which retard the binding of ZnO nanoparticles and make Gram-negative bacteria more resistant toward these particles.

ZnO nanoparticles have two major mechanisms of action that are responsible for their inhibitory action against microbial growth. The first involves the generation of free radicals, and this is considered the most common mechanism of nanoparticle-induced cell toxicity.[54] Generally, reactive oxygen-rich species, including hydroxyl ions, superoxide ions and hydrogen peroxide, are generated under UV illumination. Moreover, the annealing of ZnO nanoparticles under oxygen generates a large number of holes on the surface and consequently increases the surface area of the material. This increased surface area facilitates the absorption and diffusion of oxygen on the surface of the NPs and enhances the production of more reactive oxygen species (ROS).[55] The second pathway for the inhibitory action of ZnO nanoparticles may involve the disruption of the cell membrane through interactions between these nanoparticles and the bacterial cell membrane proteins, which in turn disrupts the cell membrane and finally leads to microbial cell death. ZnO nanoparticles can react with sulfhydryl (–SH) groups on the protein surface to form stable S–Zn bonds that deactivate the protein. Moreover, when proteins lose hydrogen ions, the membrane permeability decreases, causing cell death.[56]

Additionally, the results demonstrate PVA/PLUR/ZnO as a novel antifungal agent with potent activity against *C. albicans*, it showed a ZOI of 40.0 mm for 25 wt% ZnO and reduced the colony count to 10×10^1 after 24 h of incubation. This broad-spectrum antibacterial activity against fungi as well as both Gram-negative and Gram-positive microorganisms, including major foodborne pathogens such as *Escherichia coli*, highlights the potential of PVA/PLUR/ZnO films as candidates for active food packaging applications.

3. Conclusion

The present study demonstrates the successful synthesis of PVA/PLUR/ZnO nanocomposites based on different loadings of ZnO nanoparticles prepared via gamma irradiation as a green and novel technique. Moreover, all used materials are FDA-approved (including ZnO) as biodegradable implants that are commonly used in food-contact applications. TEM and DLS measurements confirmed that the eco-friendly ZnO nanoparticles are monodispersed and have an average diameter of 34 nm. The nanocomposite films were further characterized

Table 3. Effect of ZnO NPs (5 wt%) on the counts of different bacterial and fungal strains cultured on LB agar and sabouraud after 24 h and 4 days of incubation at 37 and 28 °C, respectively.

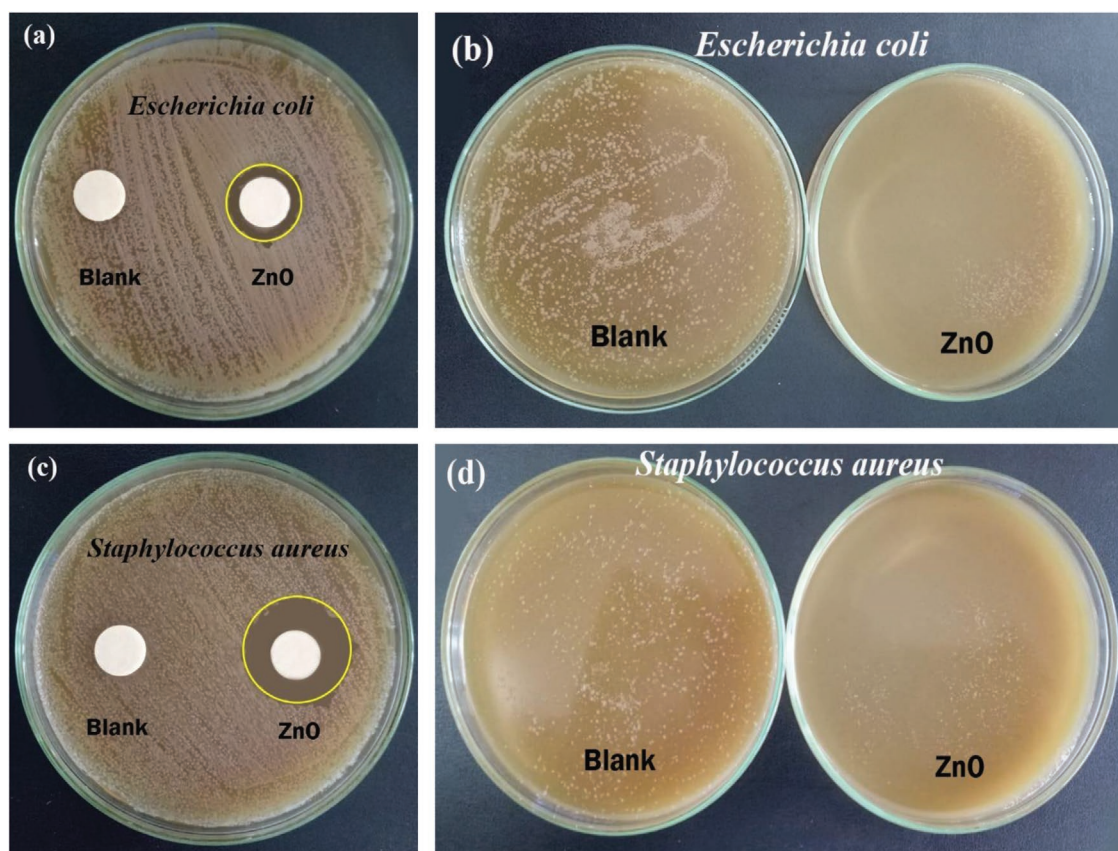| Strains	Count without ZnO NPs	Count with ZnO NPs
Escherichia coli	23×10^5	3×10^2
Bacillus subtilis	33×10^5	2×10^2
Candida albicans	29×10^5	0×10^2
Pseudomonas aeruginosa	23×10^5	4×10^2
Staphylococcus aureus	29×10^5	0×10^2

Figure 8. Inhibition zone for a) *Escherichia coli* and c) *Staphylococcus aureus* and bacterial count for b) *Escherichia coli* and d) *Staphylococcus aureus* of blank and 5 wt% ZnO.

using FT-IR and XRD techniques, and the data confirmed that the prepared ZnO nanoparticles were successfully incorporated into the PVA/PLUR matrix. The as-prepared nanocomposite films showed good morphological, thermal, barrier, and antimicrobial properties. These promising multifunctional PVA/ PLUR/ZnO materials can be used as antimicrobial polymer films with broad inhibitory activity against Gram-positive bacteria (*Bacillus subtilis* and *Staphylococcus aureus*), Gram-negative bacteria (*Escherichia coli* and *Pseudomonas aeruginosa*) and fungi (*Candida albicans*). These films offer OTR values comparable to those of food packaging materials currently available on the market, making PVA/PLUR in association with ZnO nanoparticles, a viable biodegradable alternative to commonly used packaging materials based on organic polymers, especially for food packaging applications.

4. Experimental Section

Materials: Analytical-grade zinc acetate dihydrate [Zn(CH$_3$COO)$_2$·2H$_2$O], was purchased from Oxford Laboratory, India; and was used as received. Acrylic acid was purchased from Sico Research Laboratories Pvt. Ltd., India. PVA was purchased from Loba Chemie, India and PLUR was obtained from Sigma, Germany. LB broth was purchased from Oxoid, Basingstoke, UK. Glycerol was purchased from El-Nasr Intermediate Chemicals Company, Egypt. Ultrapure deionized water was obtained from a Milli-Q system and used as a solvent. The locally isolated microbial strains were kindly provided by Laboratory of Italian Hospital, Cairo, Egypt.

Synthesis of Eco-friendly ZnO Nanoparticles: Polymer pyrolysis was used as an eco-friendly technique for preparing ZnO nanoparticles. In a typical experiment, ZnO nanoparticles were prepared using polyacrylate as precursor. The polymeric precursors loaded with ZnO nanoparticles were made via gamma irradiation of an aqueous solution of acrylic acid in the presence of zinc acetate. First, a 0.5 M solution of zinc acetate was prepared by dissolving zinc acetate in aqueous acrylic acid (acrylic acid: H$_2$O = 70:30 w/w) under stirring. Afterward, this solution was carefully bottled in hermetically sealed glass vials and sonicated prior to irradiation. Gamma irradiation was performed at the gamma radiation facility of National Center for Radiation Research and Technology (NCRRT), Egyptian Atomic Energy Authority. The irradiation process was carried out by ^{60}Co facility at dose rate 1.7 Gy h^{-1} with a total dose of 20 kGy. The obtained polyacrylates were then dried at 100 °C for 24 h and calcined at 600 °C in air for 2 h, and the final product was obtained after slowly cooling to room temperature.

Preparation of PVA/PLUR and PVA/PLUR/ZnO Films: PVA/PLUR blend functional packaging films were prepared using the solvent casting method. PVA (5 wt%) and PLUR (2 wt%) were separately dissolved in double distilled water at 60 °C, and the solution was stirred for approximately 60 min until it became homogeneous. The PVA/PLUR solutions were prepared by mixing at a blending ratio of 3:1 (wt%) for approximately 60 min with continuous stirring until a viscous homogenous liquid was formed.

For the preparation of the PVA/PLUR/ZnO films, precise weights of eco-friendly ZnO nanoparticles were added to the PVA/PLUR blend solutions to afford mass fractions of 5, 10, 15, 20, and 25 wt% ZnO. The resulting solutions were cast to PEI Petri dishes and kept in a dry atmosphere at 50 °C for approximately 24 h. After drying, the films were peeled from the Petri dishes and kept in vacuum desiccators until use.

Structural and Surface Characterization: The FT-IR spectra were acquired from 4000 to 400 cm^{-1} at a resolution of 4 cm^{-1}, using a Bruker Vertex 70 FT-IR spectrometer, Germany. XRD analyses were performed

on a Shimadzu machine (XRD-6000 series) with Cu-Kα radiation (λ = 1.54 Å), operated at 40 kV and 30 mA. XRD patterns were recorded in the range of 2θ = 4–90° (by steps of 0.02°). TEM images were acquired on a JEOL JEM-100CX instrument JEOL JEM-100CX, Japan. For TEM observations, the blended suspensions were dripped onto a carbon-coated copper grid and then dried at room temperature. TGA was performed with a TGA-50-Shimadzu thermal analyser in flowing gaseous nitrogen on ≈10–20 mg of the test materials. The temperature was increased from 30 to 600 °C at a heating rate of 10 °C min^{-1} under a nitrogen atmosphere at flow rate of 20 mL min^{-1}. The particle sizes of the prepared nanoparticles were measured by DLS, using a PSS-NICOMP particle sizer 380ZLS (PSS-NICOMP, Santa Barbara, CA, USA).

Oxygen Transmission Rate: The OTR of the nanocomposite films was determined using an OxySense 5000 series oxygen analyzer (Dallas, TX, USA). The permeation chamber is part of the OxyPerm line of oxygen analysis accessories. Measurements were carried out at 25 °C and 0% relative humidity until a steady-state OTR was reached. The output values are expressed as the OTR in [mL m^{-2} per day].

Color and Opacity of the Films: The light absorption of the films was employed in order to evaluate their transparency. To measure the absorbance of the films, the film samples were cut into rectangular pieces, which were directly mounted in the sample compartment of the spectrophotometer. The absorbance was measured using a UV–vis spectrophotometer (Jasco V560 model UV–vis spectrophotometer, Japan) by measuring percent transmittance at 600 nm. To evaluate the quality of the film's color, images in JPEG format were taken using a camera (Oppo F9 smartphone, China). Then the homogeneous areas of interest from the two images with 1000 × 1000 pixels were isolated and analyzed using MATLAB 2016 software (MathWorks, Inc., MA, USA).

Bacterial Cell Growth and Viability Testing: Bacterial strains were collected from Italian Hospital, Cairo. For routine use, the cultures were maintained on LB agar. Glycerol stock solutions were prepared and kept at −20 °C for long-term storage. In this study, seven pathogenic microorganisms were selected, including two Gram-positive bacterial pathogens (*Bacillus subtilis* and *Staphylococcus aureus*), two Gram-negative bacterial pathogens (*Escherichia coli* and *Pseudomonas aeruginosa*) and a fungus (*Candida albicans*).

For experimental purposes, bacteria were grown aerobically in 50 mL of LB broth statically at 37 °C for 24 h. The overnight culture of the bacterial suspension (10^6 CFU mL^{-1}) was inoculated by spreading on PVA/PLUR solution containing different mass fractions of ZnO nanoparticles. The antibacterial properties of the films were evaluated by monitoring ZOI and cell count.

Statistical Analysis: The data obtained in the present work are presented as the mean ± standard deviation. Statistical analysis was carried out using Statistical Package for Social Science software version 20 using one-way analysis of variance (one-way ANOVA); $p \leq 0.05$ were considered significant. Experiments were performed in triplicate with PVA/PLUR as a control.

Supporting Information

Supporting Information is available from the Wiley Online Library or from the author.

Conflict of Interest

The authors declare no conflict of interest.

Keywords

[1] M. Avella, J. J. De Vlieger, M. E. Errico, S. Fischer, P. Vacca, M. G. Volpe, *Food Chem.* **2005**, *93*, 467.

[2] D. Olmos, G. M. Pontes-Quero, A. Corral, G. González-Gaitano, J. González-Benito, *Nanomater* **2018**, *8*, 60.

[3] I. S. Tawakkal, M. J. Cran, S. W. Bigger, *J. Appl. Polym. Sci.* **2016**, *133*, 4216.

[4] A. E. Gharoy, M. H. Abbaspour-Fard, N. Shahtahmassebi, M. Khojastehpour, P. Maddah, *J. Food Process. Pres.* **2015**, *39*, 1442.

[5] L. Tamayo, M. Azócar, M. Kogan, A. Riveros, M. Páez, *Mater. Sci. Eng. C* **2016**, *69*, 1391.

[6] N. A. Al-Tayyar, A. M. Youssef, R. Al-hindi, *Food Chem.* **2019**, *310*, 125915.

[7] M. Carbone, D. T. Donia, G. Sabbatella, R. Antiochia, *J. King Saud Univ. Sci.* **2016**, *28*, 273.

[8] J. W. Rhim, H. M. Park, C. S. Ha, *Prog. Polym. Sci.* **2013**, *38*, 1629.

[9] N. F. Atta, K. M. Amin, H. A. Abd El-Rehim, A. Galal, *RSC Adv.* **2015**, *5*, 71627.

[10] V. Dhapte, N. Gaikwad, P. V. More, S. Banerjee, V. V. Dhapte, S. Kadam, P. K. Khanna, *Nanocomposites* **2015**, *1*, 106.

[11] R. Venkatesan, N. Rajeswari, *Polym. Adv. Technol.* **2017**, *28*, 20.

[12] T. Jin, D. Sun, J. Y. Su, H. Zhang, H. J. Sue, *J. Food Sci.* **2009**, *74*, 46.

[13] B. Xiang, P. Wang, X. Zhang, S. A. Dayeh, D. P. Aplin, C. Soci, D. Yu, D. Wang, *Nano Lett.* **2007**, *7*, 323.

[14] M. T. Thein, S. Y. Pung, A. Aziz, M. Itoh, *J. Sol-Gel Sci. Technol.* **2015**, *74*, 260.

[15] C. C. Lin, Y. Y. Li, *Mater. Chem. Phys.* **2009**, *113*, 334.

[16] X. Zhou, T. Shi, H. Zhou, *Appl. Surf. Sci.* **2012**, *258*, 6204.

[17] N. Lehraki, M. S. Aida, S. Abed, N. Attaf, A. Attaf, *Appl. Phys.* **2012**, *12*, 1283.

[18] H. J. Park, K. H. Lee, I. Sameera, S. W. Kim, *J. Korean Phys. Soc.* **2015**, *66*, 1422.

[19] J. N. Hasnidawani, H. N. Azlina, H. Norita, N. N. Bonnia, S. Ratim, E. S. Ali, *Procedia Chem.* **2016**, *19*, 211.

[20] A. Galal, K. M. Amin, N. F. Atta, H. A. Abd El-Rehim, *J. Alloys Compd.* **2017**, *695*, 638.

[21] A. H. Farha, S. A. Mansour, M. F. Kotkata, *J. Mater. Sci.* **2016**, *51*, 9855.

[22] Y. Q. Li, K. Yong, H. M. Xiao, W. J. Ma, G. L. Zhang, S. Y. Fu, *Mater. Lett.* **2010**, *64*, 1735.

[23] S. A. Mansour, A. H. Farha, M. F. Kotkata, *Int. J. Appl. Ceram. Technol.* **2017**, *14*, 1213.

[24] Y. Huang, L. Mei, X. Chen, Q. Wang, *Nanomater* **2018**, *8*, 830.

[25] S. H. Othman, *Sci. Procedia* **2014**, *1*, 296.

[26] B. G. Ershov, A. V. Gordeev, *Radiat. Phys. Chem.* **2008**, *77*, 928.

[27] A. Król, V. Railean-Plugaru, P. Pomastowski, M. Złoch, B. Buszewski, *Colloids Surf., A* **2018**, *553*, 349.

[28] R. Suntako, *Bull. Mater. Sci.* **2015**, *38*, 1033.

[29] Y. T. Prabhu, K. V. Rao, V. S. S. Kumar, B. S. Kumari, *Adv. Nanopart.* **2013**, *2*, 45.

[30] T. Siddaiah, P. Ojha, N. O. Kumar, C. Ramu, *Mater. Res.* **2018**, *21*, e20170987.

[31] I. Restrepo, N. Benito, C. Medinam, R. V. Mangalaraja, P. Flores, S. Rodriguez-Llamazares, *Mater. Res. Express* **2017**, *4*, 105019.

[32] M. R. El-Aassar, N. M. El-Deeb, H. S. Hassan, X. Mo, *Appl. Biochem. Biotechnol.* **2016**, *178*, 1488.

[33] S. Azizi, M. B. Ahmad, N. A. Ibrahim, M. Z. Hussein, F. Namvar, *Int. J. Mol. Sci.* **2014**, *15*, 11040.

[34] X. Y. Ma, W. D. Zhang, *Polym. Degrad. Stab.* **2009**, *94*, 1103.

[35] A. S. Roy, S. Gupta, S. Sindhu, A. Parveen, P. C. Ramamurthy, *Comp. B Eng.* **2013**, *47*, 314.

[36] X. Gong, C. Y. Tang, L. Pan, Z. Hao, C. P. Tsui, *Comp. B Eng.* **2014**, *60*, 144.

[37] J. Lee, K. J. Lee, J. Jang, *Polym. Test.* **2008**, *27*, 360.

[38] D. E. El-Nashar, N. N. Rozik, A. M. Soliman, F. Helaly, *J. Appl. Pharm. Sci.* **2016**, *6*, 067.

[39] W. G. Liu, X. C. Zhang, H. Y. Li, Z. Liu, *Comp. B Eng.* **2012**, *43*, 2209.

[40] A. Khan, S. Mehmood, M. Shafiq, T. Yasin, Z. Akhter, S. Ahmad, *Radiat. Phys. Chem.* **2013**, *91*, 138.

[41] N. M. Shamhari, B. S. Wee, S. F. Chin, K. Y. Kok, *Acta Chim. Slov.* **2018**, *65*, 578.

[42] A. Sabir, W. Falath, K. I. Jacob, M. Shafiq, N. Gull, A. Islam, M. A. Munawar, S. Zia, S. M. Khan, A. Shafeeq, M. T. Butt, *Mater. Chem. Phys.* **2016**, *183*, 595.

[43] R. Kandulna, R. B. Choudhary, *Polym. Bull.* **2018**, *75*, 3089.

[44] Y. Gutha, J. L. Pathak, W. Zhang, Y. Zhang, X. Jiao, *Int. J. Biol. Macromol.* **2017**, *103*, 234.

[45] D. Yayli, S. Turhan, F. T. Saricaoglu, *Korean Food Sci. Anim. Resour.* **2017**, *37*, 635.

[46] P. Kanmani, J. W. Rhim, *Carbohydr. Polym.* **2014**, *106*, 190.

[47] G. Chinga-Carrasco, K. Syverud, *Nanoscale Res. Lett.* **2012**, *7*, 192.

[48] D. Manley, *Manley's Technology of Biscuits, Crackers and Cookies, Manley's Technology of Biscuits, Crackers and Cookies*, Elsevier, New York **2011**.

[49] O. J. Caleb, P. V. Mahajan, F. A. Al-Said, U. L. Opara, *Food Bioprocess Technol.* **2013**, *6*, 303.

[50] S. Azizi, M. B. Ahmad, N. A. Ibrahim, M. Z. Hussein, F. Namvar, *Chin. J. Polym. Sci.* **2014**, *32*, 1620.

[51] H. Agarwal, S. Menon, S. V. Kumar, S. Rajeshkumar, *Chem-Biol. Interact.* **2018**, *286*, 60.

[52] S. M. El-Sayed, M. A. Amer, T. M. Meaz, N. M. Deghiedy, H. A. El-Shershaby, *Measurement* **2020**, *151*, 107191.

[53] A. A. Tayel, W. F. El-tras, S. Moussa, A. F. El-baz, H. Mahrous, M. F. Salem, L. Brimer, *J. Food Safety* **2011**, *31*, 211.

[54] Y. H. Leung, X. Xu, A. P. Ma, F. Liu, A. M. Ng, Z. Shen, L. A. Gethings, M. Y. Guo, A. B. Djurišić, P. K. Lee, H. K. Lee, *Sci. Rep.* **2016**, *6*, 35243.

[55] S. Paisoonsin, O. Pornsunthorntawee, R. Rujiravani, *Appl. Surf. Sci.* **2013**, *273*, 824.

[56] E. M. Azzam, M. F. Zaki, *Egypt. J. Pet.* **2016**, *25*, 153.